

Transport in metallic multi-island Coulomb blockade systems - a systematic perturbative expansion in the junction transparency

Björn Kubala¹, Göran Johansson², and Jürgen König¹

¹Institut für Theoretische Physik III, Ruhr-Universität Bochum, D-44780 Bochum, Germany

²Applied Quantum Physics, MC2, Chalmers, S-412 96 Göteborg, Sweden

(Dated: May 24, 2019)

We study electronic transport through metallic multi-island Coulomb-blockade systems. Based on a diagrammatic real-time approach, we develop a computer algorithm that generates and calculates all transport contributions up to second order in the tunnel-coupling strengths for arbitrary multi-island systems. This comprises sequential and cotunneling, as well as terms corresponding to a renormalization of charging energies and tunneling conductances. Multi-island cotunneling processes with energy transfer between different island are taken into account. We illustrate our approach with a two-island setup.

PACS numbers: 73.23.Hk, 73.40.Gk, 72.70.+m, 85.35.Gv

I. INTRODUCTION

Charging effects strongly influence the tunneling of electrons through small metallic, normal-state islands, leading to the well-known Coulomb blockade of transport at low temperatures.^{1,2,3} Early theoretical and experimental studies explored Coulomb-blockade effects in a single gated island – a so-called single electron transistor (SET) – in great detail.⁴

Soon afterwards a number of theoretical^{5,6,7,8} and experimental works also considered multi-island systems, where several islands are coupled capacitatively or by tunneling junctions (see Fig. 1). One approach^{9,10,11,12} is concerned with using one part of the multi-island system as measurement device for the residue. Serial arrays of islands^{13,14,15,16,17,18,19,20,21} have been put forward for metrological purposes: for primary thermometry¹⁶ and, operated as electron pumps, as a standard for both current and capacitance.^{17,18,19,20} For each cycle of periodically changing the gate voltages one electron is transferred through the system. The main operation of these devices is described by first-order perturbation theory in the junction conductances, known as orthodox theory for single-electron tunneling.²² Contributions from second- or higher-order processes, so-called cotunneling,^{23,24} are limiting the accuracy of the latter devices.^{17,25} In other experiments higher-order tunneling contributions are of fundamental physical interest. For instance, logarithmical temperature dependence of the conductance associated with multi-channel Kondo correlations, which govern the low-temperature transport properties of a single-electron transistor,^{26,27,28} could be explained by a second-order perturbation expansion at the resonance peak.²⁹ For large transparency of the tunnel contacts, first- and second-order perturbation theory is no longer applicable, and alternative approaches suitable to describe transport in the strong tunneling regime such as semiclassical approaches,^{30,31} real-time renormalization-group techniques,^{8,32} path-integral Monte-Carlo simulations,³³ or non-perturbative resummations within a real-time diagrammatic formulation³⁴ were put forward.

In this paper we describe a real-time diagrammatic approach to transport through multi-island systems that allows for a systematic perturbation expansion in the tunnel-coupling

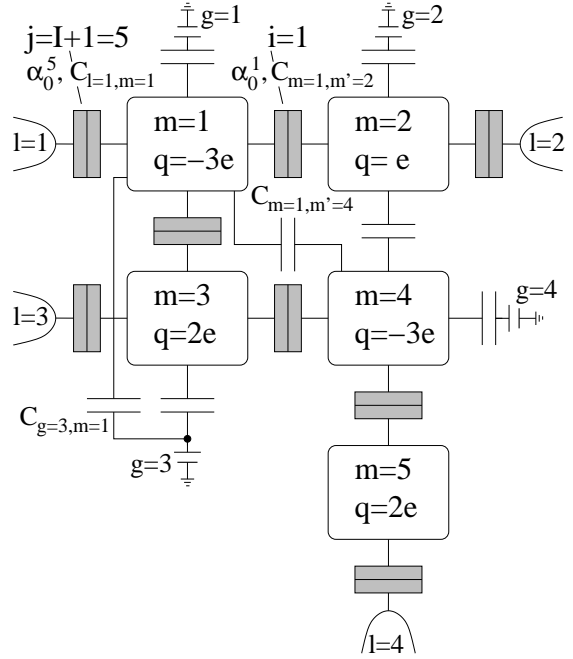


FIG. 1: An example of a multi-island geometry. The system consists of $M = 5$ islands with $I = 4$ island-island and $J = 4$ island-lead junctions. Any junction, e.g. $i = 1$, in between a pair $(m_1 = 1, m'_1 = 2)$ of islands is characterized by a transparency α_0^i (see Eqn. 11 below for definition) and a capacitance $C_{m=1,m'=2}$. Only some stray capacitances are shown in the sketch. The state of the system is given by the excess charges on the islands: $|\chi\rangle = |-3, 1, 2, -3, 2\rangle$.

strengths of the tunnel contacts. In particular, we develop a computer algorithm that generates and calculates all possible contributions to second-order transport for arbitrary multi-island systems. The theory is a generalization of a diagrammatic real-time approach that was invented for single-island devices.³⁴ In contrast to the latter, where a fully analytical treatment of first- plus second-order transport is feasible,²⁹ the large number of second-order diagrams for multi-island

systems motivates the development and use of a computer algorithm. The same idea has been used in advanced computer codes for SET networks based on orthodox theory.^{36,37}

Second-order transport includes cotunneling processes in the Coulomb-blockade regime, where sequential tunneling is suppressed. In the standard description of these cotunneling processes,^{23,24} energy denominators appear that diverge when approaching the onset of sequential tunneling. These divergencies can be removed by replacing the energy denominator with some constant²⁵ or by partial resummation of higher-order contributions.³⁵ Besides cotunneling processes, there are other second-order contributions to transport that become relevant in the regime in which sequential tunneling is not suppressed. They account for the fact that quantum fluctuations due to tunneling give rise to a renormalization of both the charging energies and the tunnel coupling strengths. This results in transport contributions that have the functional form of sequential tunneling but with renormalized system parameters. An example is the tell-tale characteristics of a multi-channel Kondo-effect at low temperature in a metallic single-electron transistor.^{27,28,29} Similar renormalization effects are also found in a diagrammatic real-time description of second-order transport through single-level quantum dots.³⁸ The virtue of the real-time diagrammatic approach employed in this paper lies in the fact that the above mentioned divergencies of energy denominators are automatically regularized, and that the renormalization effects are taken into account. It, therefore, allows for a complete and consistent evaluation of second-order transport.

Second-order transport in multi-island systems is qualitatively different from that in single-island devices. In multi-island systems, cotunneling processes in which two different islands change their charge occupation may occur. The energy conservation of the total process may be fulfilled by exciting one island on cost of the other one. This introduces a coupling between the two islands that may be of importance in devices in which one island is used as a measurement tool for the charge state of the other one, as we will discuss in more detail below. Our theory includes cotunneling involving either one or more than one island.

The outline of the paper is as follows. First, we present the extension of the real-time diagrammatic theory³⁴ to multi-island systems. Then, in Sec. III, we present the algorithmic approach to generate and evaluate all second-order contributions to transport. This includes a discussion of the applicability range of our perturbation expansion. Further details concerning calculation of diagrams and convergence properties of the perturbative expansion are included in Apps. A and B. Afterwards, we illustrate our theory by applying it to one of the simplest multi-island setup, namely that of two single-electron transistors put in parallel, Sec. IV. For this example, we discuss the physics of energy exchange between the two transistors, interpret it within a simplified picture using a $P(E)$ -description of photon-assisted tunneling, and demonstrate the virtue and the limits of this picture by comparing it with our full second-order calculation.

II. REAL-TIME DIAGRAMMICS FOR METALLIC MULTI-ISLAND SYSTEMS

A. Metallic multi-island geometries

The system we consider in this paper consists of a number M of small metallic islands as well as L leads, which are connected to some islands by J junctions (see Fig. 1). Additionally there are I junctions between the metallic islands. Accordingly with any junction $i = 1, 2, \dots, I$ we will associate the pair of islands (m_i, m'_i) it is connecting, where the order is arbitrary but fixed, thus defining a ‘direction’ for the junction. Likewise for any of the junction between leads and islands,³⁹ indexed by $j = I+1, I+2, \dots, I+J$, we define a pair (l_j, m_j) . Furthermore we have to take into account the capacitances C_{lm} between islands and leads, $C_{mm'}$ in between two islands, as well as capacitances C_{gm} to additional external gates g .

For typical samples of metallic islands the level spectrum is dense and the total charge on any island is large. Therefore not only the leads but also the islands can be considered as large equilibrium reservoirs, described by Fermi distribution functions. These equilibrium distribution functions are not influenced by tunneling processes comprising only a very small fraction of the overall number of electrons. Electron-hole excitations left behind after tunneling are quickly equilibrated - on a time scale short compared to typical times between tunneling events.

The state of our system is then described by the excess charges $\chi = \{n_1, \dots, n_M\}$ (total charge minus background charge) sitting on the M islands.

1. The Hamiltonian:

The system can be modeled by the Hamiltonian:

$$H = H_L + H_M + V + H_T = H_0 + H_T. \quad (1)$$

The noninteracting electrons in the leads and islands are described by

$$H_L = \sum_{l=1}^L \sum_{\kappa v} \tilde{\epsilon}_{\kappa v}^l a_{l \kappa v}^\dagger a_{l \kappa v}, \quad H_M = \sum_{m=1}^M \sum_{\lambda v} \epsilon_{\lambda v}^m c_{m \lambda v}^\dagger c_{m \lambda v}, \quad (2)$$

where wave vectors κ and λ numerate electron states within a given transverse channel v [Note, that the transverse channel index v includes the spin of the electrons. For ease of notation we omit subindices κ_{lv} or λ_{mv} throughout.].

Coulomb interaction of electrons is captured by $V = V(\hat{\chi})$, the electrostatic energy of a given charge state $|\chi\rangle = |n_1, n_2, \dots, n_M\rangle$. It depends in a complex way on gate and bias voltages and the resulting charges on the capacitances C_{lm} , $C_{mm'}$, and C_{gm} , respectively. A straightforward scheme to calculate this dependence, governed by classical electrostatics is given in Ref. 40. There a capacitance matrix is introduced to first calculate voltages on the islands and subsequently the

electrostatic energy. For an example of the gate and bias voltage dependence of the electrostatic energy, see the discussion of a two-island setup in Sec. IV A.

Finally charge transfer through the junctions is depicted by the tunneling Hamiltonian:

$$H_T = \sum_j \sum_{\kappa\lambda\nu} \left(T_{\kappa\lambda}^{j\nu} a_{l_j\kappa\nu}^\dagger c_{m_j\lambda\nu} e^{-i\hat{\phi}_{m_j}} + \text{c.c.} \right) + \sum_i \sum_{\lambda\lambda'\nu} \left(T_{\lambda\lambda'}^{i\nu} c_{m_i\lambda\nu}^\dagger c_{m_i'\lambda'\nu} e^{-i(\hat{\phi}_{m_i'} - \hat{\phi}_{m_i})} + \text{c.c.} \right), \quad (3)$$

where $T_{\kappa\lambda}^{j\nu}$ and $T_{\lambda\lambda'}^{i\nu}$ are tunneling matrix elements for junctions j , respectively i and $\exp(\pm i\hat{\phi}_{m_{j/i}})$ is a charge shift operator, acting on the charge state $|\chi\rangle$ described above.⁴¹

Involving a phase operator $\hat{\phi}_m$ as a canonical conjugate to the charge operator \hat{N}_m of the island m , i.e., $[\hat{\phi}_m, \hat{N}_m] = i$, these operators $\exp(\pm i\hat{\phi}_m)$ changes the excess particle number on the island m as $n_m \rightarrow n_m \pm 1$ for each tunneling process accordingly.

B. Diagrammatic technique

In this section we generalize the diagrammatic technique developed in Ref. 34 for a single SET to study multi-islands systems as described by Eqns. 1-3 above. A short overview over the derivation is given, while the reader is referred to Refs. 29,34,42 for more details. In subsection II B 5 we explicitly discuss differences between single and multi-island case.

1. The current:

One of the central objects of our theoretical description is the probability P_χ , to find the multi-island system in a certain state $|\chi\rangle = |n_1, n_2, \dots, n_M\rangle$ in charge space. Experimentally accessible quantities such as the average charge of a certain island follow directly from this probability. The other quantity, we will mainly be focused on, is the current flowing through junction j into reservoir l_j , given by the change in the number of particles:

$$I_l(t) = e \frac{d}{dt} \langle \hat{N}_{l_j}(t) \rangle = e \sum_{\kappa\lambda\nu} \left[T_{\kappa\lambda}^{j\nu} \langle (a_{l_j\kappa\nu}^\dagger c_{m_j\lambda\nu} e^{-i\hat{\phi}_{m_j}})(t) + \text{c.c.} \rangle \right]. \quad (4)$$

Note that the current operator has a similar structure as the tunneling Hamiltonian H_T .

2. Time evolution of operators:

The non-equilibrium time evolution of the charge degrees of freedom is described by the expectation value of the (diag-

onal) density matrix:

$$\begin{aligned} P_\chi(t) &= \langle (|\chi\rangle\langle\chi|)(t) \rangle \\ &= \text{Tr} \left(\rho_0 T^+ e^{i \int_{t_0}^t dt' H_T(t')_I} |\chi\rangle\langle\chi| T^- e^{-i \int_{t_0}^t dt' H_T(t')_I} \right) \\ &= \text{Tr} \left(\rho_0 \sum_{s=0}^{\infty} (-i)^s \int_K dt'_1 \int_K^{t'_1} dt'_2 \dots \int_K^{t'_s} dt'_s \right. \\ &\quad \left. \times T^K [H_T(t'_1)_I H_T(t'_2)_I \dots H_T(t'_s)_I |\chi\rangle\langle\chi|] \right) \quad (5) \end{aligned}$$

Here we replace time-ordering T^+ and anti-time-ordering operators T^- by introducing integration $\int_K dt'$ along the Keldysh-contour with ‘times’ t' running forward from t_0 to t and backward from t to t_0 (see Fig. 2). The ordering of times $t'_1 < t'_2 < \dots < t'_s$ is with respect to this Keldysh-contour with the Keldysh-time-ordering operator T^K arranging the operators in the tunneling Hamiltonian in proper order. $H_T(t)_I$ denotes the tunneling part of the Hamiltonian (Eqn. 1) in interaction representation with respect to H_0 .

Due to the separation of fermionic and charge degrees of freedom the Hamiltonian H_0 , including interaction through the charging energy $V(\chi)$, is bilinear only in electron operators. Thus we can apply Wick’s theorem and perform the trace over these degrees of freedom by contracting tunneling vertices in pairs.

In fact, there are two independent contraction lines for each vertex, as each of the two electron operators $a_{l_j\kappa\nu}^\dagger/a_{l_j\kappa\nu}$ and $c_{m_j\lambda\nu}^\dagger/c_{m_j\lambda\nu}$ constituting a tunneling vertex is connected to another matching operator $a_{l_j\kappa\nu}/a_{l_j\kappa\nu}^\dagger$ and $c_{m_j\lambda\nu}/c_{m_j\lambda\nu}^\dagger$, not necessarily both of these being part of the same tunneling vertex. However in the limit of large transverse channel number ‘simple loop’ configurations dominate and we can represent contractions by one (directed⁴³) double tunneling line between pairs of vertices. Readers may refer to Figs. 2 and 10 of Ref. 34 for an illustration.

A realization of a resulting diagram is shown in Fig. 2, where certain physical processes can be identified with parts of the diagram. The leftmost part shows explicitly, how the charge state is changed by a tunneling process across junction j . Processes with several tunneling lines at a time t correspond to higher order processes like cotunneling.

3. Generalized master equation:

From these diagrams for the time evolution of the density matrix a formally exact master equation can be derived:

$$\frac{d}{dt} P_\chi(t) = \sum_{\chi' \neq \chi} \int_{t_0}^t dt' [P_{\chi'}(t') \Sigma_{\chi',\chi}(t',t) - P_\chi(t') \Sigma_{\chi,\chi'}(t',t)], \quad (6)$$

where the central object needed as input is the full quantum mechanical transition rate $\Sigma_{\chi',\chi}(t',t)$ from a state χ' at time t' to state χ at time t . This rate is the sum over all irreducible (see Fig. 2) diagrams and corresponds to the self-energy of a

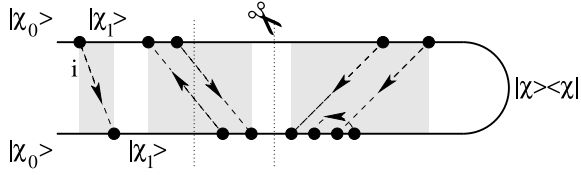


FIG. 2: Diagram describing the time evolution of the islands' density matrix with sequential tunneling, cotunneling (two tunneling lines at a time) and higher order processes (from left to right). The diagram is reducible, i.e., it can be cut at a certain time without cutting a tunneling contraction line. Summing irreducible parts (shaded) yields the self-energy. In the leftmost part a tunneling process through junction i in between a pair of islands (m_i, m'_i) changes the state of the island on the upper branch from $|\chi_0\rangle = |n_1, n_2, \dots, n_{m_i}, \dots, n_{m'_i}, \dots, n_M\rangle$ to $|\chi_1\rangle = |n_1, n_2, \dots, n_{m_i} - 1, \dots, n_{m'_i} + 1, \dots, n_M\rangle$.

Dyson-equation for the full propagator of the system. After Laplace transforming, the stationary distribution P_χ of charge states is found by:

$$0 = \sum_{\chi'} P_{\chi'} \Sigma_{\chi', \chi}, \text{ with } \Sigma_{\chi', \chi} = i \int_{-\infty}^0 dt' \Sigma_{\chi', \chi}(t', 0). \quad (7)$$

In a similar manner as for the density matrix a diagrammatic representation for the expectation value of the current is found. The current operator becomes manifest in any such diagram as an additional external vertex (cf. Eqns. 3 and 4) at the (rightmost) time t . As above *partial* self-energies can be defined:

$$\Sigma_{\chi', \chi}(t', t) = \sum_j \left\{ \Sigma_{\chi', \chi}^{j+}(t', t) + \Sigma_{\chi', \chi}^{j-}(t', t) \right\}. \quad (8)$$

Here $\Sigma_{\chi', \chi}^{j+}$ includes all those diagrams contributing to $\Sigma_{\chi', \chi}$ with the rightmost vertex on the upper propagator and rightmost contraction line describing tunneling out of lead l_j through junction j as well as diagrams with rightmost vertex on the lower propagator and the rightmost process describing tunneling into lead l_j ; correspondingly summing the remaining self-energy diagrams with rightmost tunneling through junction j defines $\Sigma_{\chi', \chi}^{j-}$.

The stationary current then follows as:

$$I_{l_j} = -ie \sum_{\chi, \chi'} P_{\chi'} \Sigma_{\chi', \chi}^{j+} = ie \sum_{\chi, \chi'} P_{\chi'} \Sigma_{\chi', \chi}^{j-}. \quad (9)$$

4. Diagrammatic rules:

Identification of terms of the sums in Eqn. 5 with diagrams leads to a set of rules (for details see Ref. 34) for calculating the value of a certain realization of a diagram. Here we will give these rules in the form most convenient for calculating the Laplace-transform of the self-energy, which allows calculation of stationary probabilities and current via Eqns. 7 and 9:

(1) Draw all topologically different diagrams with tunneling lines and choose junction and direction for each line. Assign energies $V(\chi)$ to propagators, ω_r to tunneling lines.

(2) Each segment from $t_s \leq t \leq t_{s+1}$ gives a factor $[\Delta E_s + i\eta]^{-1}$, where ΔE_s is difference of left-going minus right-going energies (including the energies ω_r of tunneling lines).

(3) Each tunneling line gives a rate function $\alpha^{j/i\pm}(\omega_r)$ – as defined below – for the direction of the tunneling line across junction j/i going backward/forward with respect to the Keldysh contour.

(4) There is a prefactor (-1) for each internal vertex on the backward propagator.

(5) Integrate over the energies ω_r of tunneling lines.

The golden-rule rate $\alpha^{j\pm}$ ($\alpha^{i\pm}$ correspondingly) stems from implicit integration over the energy of one of the double tunneling lines

$$\alpha^{j\pm}(\omega) = \int dE \alpha_0^j f_{l_j}^{\pm}(E + \omega) f_{m_j}^{\mp}(E) = \pm \alpha_0^j \frac{\omega - \mu_{l_j}}{e^{\pm\beta(\omega - \mu_{l_j})} - 1}, \quad (10)$$

where $f_{l/m}^+$ is the Fermi distribution function of lead l or island m and $f_m^- = 1 - f_m^+$. Hereby assuming constant tunneling matrix elements $T^{jv} = T_{\kappa\lambda}^{jv}$ as well as a constant temperature $k_B T = 1/\beta$ across the sample and neglecting energy dependencies of the density of states $N^{l/m}v(E)$, each junction j is characterized by a single parameter:

$$\alpha_0^j = \sum_v |T^{jv}|^2 N^{m_j v}(0) N^{l_j v}(0) = \frac{\hbar}{4\pi^2 e^2} \frac{1}{R_j} = \frac{R_K}{4\pi^2 R_j}, \quad (11)$$

related to the tunneling resistance R_j of the junction.

5. Diagrams for single and multiple islands:

The formalism of real-time diagrammatics as presented in the previous section is applicable to the study of arbitrary multi-island system, as defined by the Hamiltonian Eqns. 1-3. Hitherto derivation and application was mainly concerned with the case of a single island (see e.g. Ref. 42 and references therein) and one study of two islands in series.⁸ Therefore this section is devoted to a brief summation of differences between single and multi-island case.

Virtually the entire formalism of real-time diagrammatics translates from single to multi-island case by switching over from one variable of interest, the charge on the island n , to the M -tuple $\chi = n_1, n_2, \dots, n_M$ of charges on all the M islands. This extension of state space has non-trivial effects only for the practical application of the method, but not for general scheme and derivation. Complications for the multi-island as compared to the single-island case arise due to the non-trivial electrostatic charging energies, numerous tunneling processes mediating between any two charge states, and most importantly the exponentially increasing number of charge states as the number of islands grows.

III. ALGORITHMIC DIAGRAMMATICS

As for a general multi-island system a closed analytic solution seems unattainable, we set up and use in the following an automatized, computer-based numerical approach.

A. Algorithmic scheme

From our discussion above we learned about the essential steps in our problem: Solving the electrostatics delivers the energy terms, needed for calculating rates of certain processes, which allow to find stationary solutions of the rate equations. In this section we present the automatization of this process, where the by far most intricate part is the actual calculation of rates. This includes the automatic generation and calculation of real-time diagrams.

The first step in our scheme is the restriction to a finite charge state space. This subspace will include all states within a few $k_B T$ around the classical ground-state and additionally all states reachable by simple tunneling events from these classically occupied states. Note that this choice can be self-consistently checked from the resulting occupation probabilities. For all these states the electrostatic energies $V(\chi)$, which also depend on gate and bias voltages, are calculated according to the method presented in Ref. 40.

B. Transition rates

We gain the rates entering Eqns. 7 and 9 up to second order in tunneling by generating and calculating all self-energies diagrams with one or two contraction lines. The scheme of generating all diagrams of a certain order is presented in the following for second order diagrams, first order being trivial, whereas higher-order diagrams, although easily generated, are considerably harder to calculate and will not be considered below.

1. Generating diagrams:

Starting with a certain state χ' of our chosen subspace of charge states for both, upper and lower branch of the Keldysh-contour (see Ref. 34 for a discussion of the diagonality of Σ) the following steps were implemented:

A *first* (i.e. leftmost) vertex v_1 is placed on either upper or lower branch, a junction j_1/i_1 as well as a direction for the tunneling event is chosen. This determines the charge state⁴⁴ on both branches in between vertices v_1 and v_2 and consequently the energy terms determining the ‘free’ propagation, governed by H_0 and the tunneling line energy ω_1 . For the *second* vertex v_2 the same choices can be independently made, as it is not contracted with the first vertex. (Such a connection would result in a diagram, reducible to two first order blocks, thus not being part of the irreducible second order self-energy.) The *third* vertex, however, is connected to either one of the vertices v_1 or v_2 , inheriting whereby junction

and direction of the tunneling event, whereas position on upper or lower branch is free to choose. This is also the only freedom of choice left for the last vertex, which is combined with the remaining tunneling line. Just as at the first vertex, charge states have to be changed according to the tunneling processes at the vertices all along the propagator up to the rightmost final state χ , which is the same on upper and lower propagator.

Estimating the number of diagrams allows some gauge of the complexity of the problem. For each charge state (for low temperatures three per island, resulting in a total of 3^M) there are $2^4 \times [2(J+I)]^2 \times 2$ second order diagrams. Here the first factor stands for upper/lower branch for each vertex, the second results from vertices v_1 and v_2 for choosing junction and direction of tunneling, while the last factor stems from combining vertices into pairs.

For each of these diagrams an analytical integral expression is immediately given by the diagrammatic rules, discussed above. Evaluation of these expressions to a numerical value is discussed in App. A.

C. Stationary state solutions

The value of any first/second order diagram is then added to the appropriate matrix element of the self-energy matrix $\Sigma_{\chi',\chi}^{(1/2)}$, where indices χ', χ are initial and final charge state of the diagram.

All diagrams required for calculating currents are already created within this scheme by identifying the rightmost tunneling vertex with an external current operator. Accordingly adding (with the proper sign) the values of diagrams, which last vertex involves junction j , yields $\Sigma_{\chi',\chi}^{j\pm(1/2)}$.

$\Sigma_{\chi',\chi}^{(1/2)}$ constitute the first terms of an expansion of the self-energy in powers of α_0 :

$$\Sigma_{\chi',\chi} = \sum_{k=1}^{\infty} \Sigma_{\chi',\chi}^{(k)}. \quad (12)$$

Expanding the probabilities $P_\chi = \sum_{k=0}^{\infty} P_\chi^{(k)}$ correspondingly, we find from the stationary rate equation in first and second order:

$$0 = \sum_{\chi'} P_{\chi'}^{(0)} \Sigma_{\chi',\chi}^{(1)} \quad \text{and} \quad 0 = \sum_{\chi'} P_{\chi'}^{(0)} \Sigma_{\chi',\chi}^{(2)} + \sum_{\chi'} P_{\chi'}^{(1)} \Sigma_{\chi',\chi}^{(1)}, \quad (13)$$

which finally gives solutions for $P_{\chi'}^{(0)}$ and $P_{\chi'}^{(1)}$. For first and second order current⁴⁵, we likewise find:

$$I_j^{(1)} = -ie \sum_{\chi,\chi'} P_{\chi'}^{(0)} \Sigma_{\chi',\chi}^{j+(1)} \quad (14)$$

$$I_j^{(2)} = -ie \sum_{\chi,\chi'} \left(P_{\chi'}^{(0)} \Sigma_{\chi',\chi}^{j+(2)} + P_{\chi'}^{(1)} \Sigma_{\chi',\chi}^{j+(1)} \right). \quad (15)$$

Thus we derived a scheme to calculate experimental accessible quantities for an arbitrary multi-island geometry, namely the average current in any lead.

D. Limits of the approach

There are both practical and fundamental limits of the approach presented above. As the number of charge states, and consequently the number of diagrams to calculate grows rapidly with the number of islands, a straightforward simulation of some interesting existing experimental applications^{17,46} using long arrays of islands (7 – 100 islands) is practically infeasible. Similarly, including higher than second-order contributions would involve more complex integral expressions that complicates the numerics considerably.

The fundamental limit deals with the question of convergence of the perturbative expansion. As we derive in App. B, the inequality $\max\{k_B T, |\Delta - \mu_j|\} > |\sigma(\Delta)|$ has to be fulfilled for tunneling across any junction j . Here $|\Delta - \mu_j|$ is the distance to resonance for a tunneling process across junction j with chemical potential difference μ_j and $\sigma(\Delta)$ is the self-energy, characterizing the spectral density of the level into which tunneling occurs at energy Δ . This incorporates renormalization of level position as well as a finite lifetime width, as reflected in real and imaginary part of the self-energy. We elaborate on this statement in App. B, where we analyze the example of a single SET by comparison to a non-perturbative approach.

IV. AN EXAMPLE: TWO PARALLEL SINGLE-ELECTRON TRANSISTORS

To give an example we will now apply our method to calculate transport through two single-electron transistors (SETs), where the two islands are capacitively coupled to each other, see Fig. 3. This system was studied experimentally e.g. in Refs. 10,47. The capacitive interaction implies that a change of the charge state of one SET will change the effective gate voltage of the other, which will lead among other things to a broadening of the charge state transitions as described in Ref. 10. This is an effect visible already in first order of the tunneling conductances. The second-order contributions include cotunneling in each SET separately, but also second-order processes in which both SETs are involved. For the latter, the energy gained in a tunneling process in one SET can be used to excite the other SET to a charge state not accessible for first-order transitions. This results effectively in an energy exchange between the two islands, a feature that is qualitatively new as compared to the single-island case or first-order transport in multi-island systems. One may try to simulate this energy transfer in a simplified picture of photon-assisted first-order tunneling in the second SET coupled to a energy-providing photon bath that represents electrostatic fluctuations by tunneling processes in the first SET. This simplified approach and the effect of the energy-transfer processes on the transport characteristics will be described in more detail below. The advantage of this approach is its feasibility and compact analytical results. The disadvantage is that it relies on several approximations, and its applicability range is unclear. This question can be answered, though, by our full-fledged

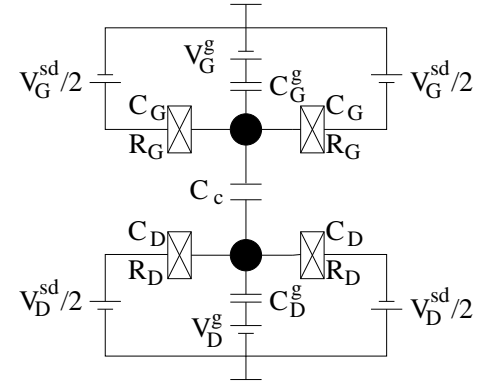


FIG. 3: Two capacitively coupled SETs. The upper one is the noise generator, and the lower the quantum noise detector.

second-order transport calculation. By comparing the results of both approaches we are able to define the range of parameters beyond which the simplified picture loses its reliability.

A. Setup

The system consists of two metallic islands (called *noise generator* and *detector* as explained below), each connected to a separate source and drain lead, see Fig. 3. Each junction is generally described by a capacitance and a tunnel resistance, as discussed in Sec. II. For simplicity we here assume that for each island the connection to source and drain is symmetric, and also that the source-drain voltage is applied symmetrically. Note, that we change our notation compared to the general setup in II A in order to make the association with the noise *generating* and *detecting* part more transparent. We denote the generator/detector junction capacitances C_G/C_D , the resistances R_G/R_D , and the applied source-drain voltages $V_G^{\text{sd}}/V_D^{\text{sd}}$. Furthermore the working point of the generator/detector SET is controlled by gate voltages (V_G^g/V_D^g) applied across the gate capacitances (C_G^g/C_D^g). The two islands are coupled through the coupling capacitance C_c .

Following Refs. 40 and 10 we find the electrostatic energy of our system. This is most straightforwardly described introducing the sum capacitances of the two islands

$$C_{G/D}^{\Sigma} = 2C_{G/D} + C_{G/D}^g + C_c,$$

the rescaled charging energies

$$E_G = \frac{e^2}{2(C_G^{\Sigma} - C_c^2/C_G^{\Sigma})}, \quad E_D = \frac{e^2}{2(C_D^{\Sigma} - C_c^2/C_D^{\Sigma})},$$

the interaction energy

$$E_{\text{int}} = \frac{e^2 C_c}{C_G^{\Sigma} C_D^{\Sigma} - C_c^2},$$

and also the dimensionless gate charges $n_x^{G/D} = C_{G/D}^g V_{G/D}^g / e$.

Then the electrostatic part of the Hamiltonian reads

$$\begin{aligned} V(n_G, n_D) = & E_G(n_G - n_x^G)^2 + E_D(n_D - n_x^D)^2 \\ & + E_{\text{int}}(n_G - n_x^G)(n_D - n_x^D). \end{aligned} \quad (16)$$

B. The noise detector SET

To illustrate the effect of photon-assisted tunneling clearly we consider our setup biased so that sequential tunneling is blocked in one of the SETs (the *noise detector*). This is done by gating $n_x^D < 1/2$ such that the Coulomb energy difference $\Delta = E_D(1 - 2n_x^D)$ between the ground state $n_D = 0$ and first excited state $n_D = 1$ is larger than temperature and applied bias $\Delta > \{eV_D^{\text{sd}}/2, k_B T\}$. Neglecting the coupling to the other SET, the dc-current through the detector is given by cotunneling

$$I_{\text{cot}}^D = e \frac{eV_D^{\text{sd}}}{h} \frac{1}{24\pi^2} \left(\frac{R_K}{R_D} \right)^2 \frac{(eV_D^{\text{sd}})^2 + (2\pi k_B T)^2}{\Delta^2}, \quad (17)$$

where we disregarded cotunneling through the state $n_D = -1$. We will find that the current induced by photon-assisted tunneling can be made orders of magnitude larger than I_{cot}^D .

C. The noise generator SET

The other SET (the *noise generator*) is biased such that a substantial current is produced by sequential tunneling, but for simplicity we keep the bias low enough so that only two charge states are involved. To be specific $n_x^G \approx 1/2$, and $eV_G^{\text{sd}}/2 < 2E_G$. The current through the noise generator SET is

$$I_{\text{seq}}^G = e \frac{eV_G^{\text{sd}}}{4h} \frac{R_K}{R_G} \left(1 - e^{-eV_G^{\text{sd}}/2k_B T} \right)^{-1}. \quad (18)$$

Each electron tunneling in the forward direction will gain the energy $eV_G^{\text{sd}}/2$ from the applied bias. Generally the electron will dissipate its excess energy on the island or in the reservoirs, but in our setup there is also the possibility to give the energy to a tunnel event in the detector SET.

D. The effect of interaction

The low-frequency effect of the interaction between the SETs can be described as an effective gate charge determined by the charge state of the other SET

$$n_{x,\text{eff}}^G(n_D) = n_x^G - \frac{C_c}{C_D^{\Sigma}}(n_D - n_x^D),$$

and

$$n_{x,\text{eff}}^D(n_G) = n_x^D - \frac{C_c}{C_G^{\Sigma}}(n_G - n_x^G),$$

as discussed in, e.g., Ref. 10 and 12. We want to minimize this effect, in order to clearly show photon-assisted tunneling. That means choosing the detector bias low enough so

that sequential tunneling is exponentially suppressed for both effective gate charges $n_{x,\text{eff}}^D(0)$ and $n_{x,\text{eff}}^D(1)$.

We will now estimate analytically the detector current due to photon-assisted sequential tunneling, driven by photons emitted from the generator with an energy higher than the Coulomb gap of the detector. We can then compare these analytical estimates with the numerical results from our algorithmic diagrammatics. We use $P(E)$ -theory,⁴⁸ considering the noise generator SET as the environment of the noise detector SET.

The function

$$P(\varepsilon) = \frac{1}{h} \int_{-\infty}^{\infty} dt \exp \left(J(t) + i \frac{\varepsilon}{\hbar} t \right), \quad (19)$$

expresses the probability of exchanging the energy ε with a certain environment in a single tunnel event. Here the function

$$\begin{aligned} J(t) &= \langle [\hat{\phi}(t) - \hat{\phi}(0)] \hat{\phi}(0) \rangle = \\ &= \frac{E_{\text{int}}^2}{\hbar^2} \int_{-\infty}^{\infty} d\omega \frac{S_N^G(\omega)}{\omega^2} (e^{-i\omega t} - 1), \end{aligned} \quad (20)$$

is given by the correlator of the phase-fluctuations on the detector island induced by the electron number fluctuations on the generator island. To simplify the analysis we approximate the fluctuations to be Gaussian. Then their asymmetric noise spectral density is given by

$$S_N^G(\omega) = \int_{-\infty}^{\infty} dt e^{-i\omega t} \langle \delta \hat{N}_G(t) \delta \hat{N}_G(0) \rangle. \quad (21)$$

We want to calculate the photon-assisted rate for an electron to tunnel onto the detector island

$$\begin{aligned} \Gamma_{01}^{D\pm} &= \frac{1}{h} \frac{R_K}{R_D} \int_{-\infty}^{\infty} \int_{-\infty}^{\infty} d\varepsilon d\varepsilon' f(\varepsilon) [1 - f(\varepsilon' - \Delta_{\pm})] P(\varepsilon - \varepsilon') \\ &= \frac{1}{h} \frac{R_K}{R_D} \int_{-\infty}^{\infty} d\varepsilon \frac{\varepsilon P(-\varepsilon - \Delta_{\pm})}{1 - e^{-\varepsilon/k_B T}}, \end{aligned} \quad (22)$$

where $\Delta_{\pm} = \Delta \pm eV_D^{\text{sd}}/2$, and Δ_{\pm} is the effective energy gap for an electron tunneling onto the island from the right/left lead. Thus we need $P(\varepsilon)$ for $\varepsilon < -\Delta_{\pm}$ indicating the probability to absorb an energy larger than Δ_{\pm} from the environment (see Fig. 4). In this regime, noting that $\Delta_{\pm} \gg E_{\text{int}}$ and using the short time expansion $e^{J(t)} = 1 + J(t)$ we can approximate⁴⁹

$$P(\varepsilon) = \frac{E_{\text{int}}^2}{h} \frac{S_N^G(\varepsilon)}{\varepsilon^2}, \quad \varepsilon \ll -E_{\text{int}}. \quad (23)$$

In the relevant frequency regime and at zero temperature the generator SET noise spectrum is^{50,51,52}

$$S_N^G(\varepsilon) = \frac{1}{\hbar} \frac{\Gamma(\varepsilon)}{4\Gamma(0)^2 + \varepsilon^2}, \quad (24)$$

where

$$\Gamma(\varepsilon) = \frac{1}{2\pi} \frac{R_K}{R_G} \left[\frac{eV_G^{\text{sd}}}{2} + \varepsilon \right], \quad |\varepsilon| < \frac{eV_G^{\text{sd}}}{2}. \quad (25)$$

Furthermore $S_N^G(\varepsilon) = 0$ for $\varepsilon < -eV_G^{\text{sd}}/2$, which is related to the fact that one cannot extract more energy from a single tunnel event than what is given by the bias voltage.

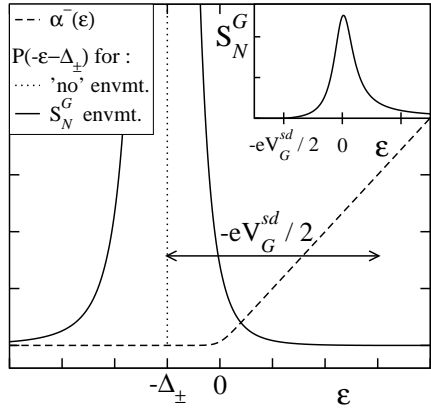


FIG. 4: Sketch of functions relevant to calculation of the photon-assisted tunneling rate (Eqn. 22). Without energy exchange with the environment ($P(\epsilon)$ is δ peaked – dotted line) the photon-assisted rate is given by the rate function α^- (broken line) at the effective energy gap Δ_{\pm} . Coupling to the noise generator SET changes $P(\epsilon)$ (solid line) and the rate is given by the integration in Eqn. 26. The inset shows the asymmetric charge noise of an SET as calculated in Ref. 52

We thus find the photon-assisted rates for electrons to tunnel onto the detector island across the right/left junction (cf. Fig. 4):

$$\Gamma_{01}^{D\pm} = \frac{1}{2\pi\hbar R_D} \int_0^{eV_G^{sd}/2-\Delta_{\pm}} d\epsilon \frac{E_{int}^2}{(\epsilon + \Delta_{\pm})^2} \frac{\epsilon\Gamma(-\epsilon - \Delta_{\pm})}{4\Gamma(0)^2 + (\epsilon + \Delta_{\pm})^2}. \quad (26)$$

Here the lower limit of the integral comes from putting temperature to zero in Eqn. (22) and the upper limit from the fact that $P(\epsilon) = 0$ for $\epsilon < -eV_G^{sd}/2$. Making the generator bias substantially larger than the detector gap ($eV_G^{sd} \gg 2\Delta_{\pm}$), we find the approximate photon-assisted rates

$$\Gamma_{01}^{D\pm} = \frac{eV_G^{sd}}{48\pi^2\hbar} \frac{R_K}{R_D} \frac{R_K}{R_G} \frac{E_{int}^2}{\Delta_{\pm}^2} f(2\Gamma(0)/\Delta_{\pm}), \quad (27)$$

where

$$f(x) = \frac{3}{x^3} \left(\pi - 2 \arctan \frac{1}{x} + x \ln(1 + x^2) - 2x \right). \quad (28)$$

We note that these rates are proportional to the bias voltage of the noise generator. If the detector gap is not too small we have $\Gamma(0) \ll \Delta_{\pm}$ which implies $x \ll 1$ and $f(x)$ approaches the limit $f(0) = 1$. For simplicity we assume this limit from here on. The relaxation rates of the detector are

$$\Gamma_{10}^{D\pm} = \frac{R_K}{R_D} \frac{\Delta_{\pm}}{\hbar}, \quad (29)$$

and accordingly the probability to find the detector in its excited state is

$$\begin{aligned} P_1^D &= \frac{\Gamma_{01}^{D+} + \Gamma_{01}^{D-}}{\Gamma_{10}^{D+} + \Gamma_{10}^{D-}} = \frac{R_K}{R_G} \frac{eV_G^{sd} E_{int}^2}{48\pi^2(\Delta_+ + \Delta_-)} \left(\frac{1}{\Delta_+^2} + \frac{1}{\Delta_-^2} \right) \approx \\ &\approx \frac{R_K}{R_G} \frac{eV_G^{sd} E_{int}^2}{48\pi^2 \Delta^3}, \end{aligned} \quad (30)$$

and the photon-assisted tunneling (PAT) detector current (assuming $eV_D^{sd} \ll \Delta_{\pm}$)

$$I_{pa}^D = e(P_1^D \Gamma_{10}^{D+} - P_0^D \Gamma_{01}^{D+}) \approx e \frac{R_K}{R_D} \frac{R_K}{R_G} \frac{eV_G^{sd} eV_D^{sd} E_{int}^2}{32\pi^2 \hbar \Delta^3}. \quad (31)$$

Comparing this with the standard cotunneling current in the detector, given in Eqn. (17),

$$\frac{I_{pa}^D}{I_{cot}^D} = \frac{3}{4} \frac{R_D}{R_G} \frac{eV_G^{sd}}{\Delta} \left(\frac{E_{int}}{eV_D^{sd}} \right)^2, \quad (32)$$

we find that the photon-assisted detector current can be made substantially larger than the usual cotunneling current by using high resistance tunnel junctions in the detector and a weak detector bias.

E. Results of diagrammatic technique

With the diagrammatic technique developed above, we have a method at our disposal for analyzing the complete two-island system on an equal footing. I.e., we do not perform a separation into detector and noisy environment as before. In particular, we can study the mutual influence of the two SETs also for the strong coupling case.

In the following, we will nonetheless focus on the weak coupling case; here we can clearly show the effects of PAT and sensibly compare to the results of $P(E)$ -theory (Eqn. 31). Low frequency effects, as described by the effective gate charges and back-action are all intrinsically included in the calculation, but parameters are chosen to minimize these.

Figure 5 (solid lines) shows current in the detector SET upon changing the bias on the generator SET for 4 different sets of sample parameters and gating. The detector is gated close to degeneracy point, i.e., $n_{x,eff}^G(n_D = 0) = 0.5$, as the detector is set preferentially unoccupied in the Coulomb blockade region. The detector is to remain in this blockade regime, independent of the generator's charge state. To achieve considerable, experimentally detectable, current through the detector, we must not be 'too deep' in Coulomb blockade. Hence, we move from a region of well defined blockade in curve A of Fig. 5 to a 'mixed' regime in curve D by changing gating (and coupling). The exact parameters are given in the captions of Fig. 5.

For *small driving* of the generator, we find the standard cotunneling current in the detector SET. The cotunneling current shown in Fig. 5 (dotted horizontal lines for curves A–C) is calculated for a single SET with effective gating $n_{x,eff}^D(n_G)$, weighted with the probabilities for the two generator states $P(n_G = 0) \approx 1/2 \approx P(n_G = 1)$.

For *strong driving* the condition for PAT above is fulfilled (i.e. $eV_G^{sd} \gg 2\Delta_{\pm}$) and we find the detector current increasing proportional to the driving voltage of the generator (cf. Eqn. 27). For the curves A and B we find the slope as predicted by $P(E)$ -theory (Eqn. 31, dashed lines in A–C). For curves C and D we do not meet all assumptions made in the derivation of the PAT rates. Consequently PAT and low

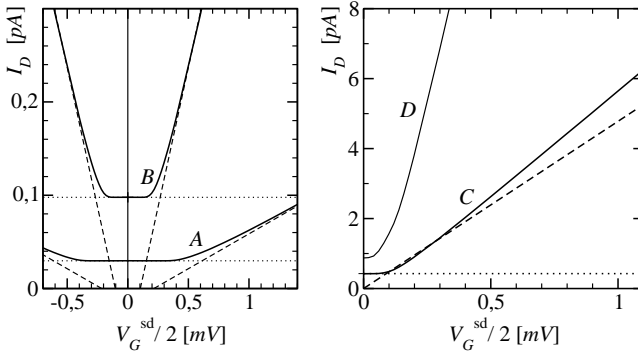


FIG. 5: Results of the diagrammatic technique for the generator/detector setup (solid lines) compared to standard cotunneling (dotted lines) and photon assisted current with slope as predicted from $P(E)$ -theory (dashed lines, x-intercepts fitted). All curves at 25mK , $eV_D^{\text{sd}} = 0.5k_B K$, and $n_{x,\text{eff}}^G(n_D = 0) = 0.5$ with $\alpha_0^j = 0.01$ for each junction; $E_G = 10k_B K$, $E_D = 10k_B K$ for A–C and $5k_B K$ for D, $E_{\text{int}} = 0.5k_B K$ for A–C and $1k_B K$ for D. n_x^D as follows: A — 0.3, B — 0.4, C — 0.45, D — 0.4.

frequency interaction effects intermingle in a complex manner and the result deviates from Eqn. 31. For D the coupling is chosen so strong, that also back-action effects are relevant, i.e., a meaningful definition of effective energy gaps and, therefore, comparison to PAT and standard cotunneling results is not possible anymore.

As the photon assisted rate was calculated assuming strong generator driving only, the crossover between standard cotunneling and PAT is not properly described. The results of our full theory (solid lines in Fig. 5) show, however, the expected behavior — an onset of PAT (i.e., the x-intercept of the dashed lines in Fig. 5 A and B), where $eV_G^{\text{sd}} \approx \Delta_{\pm}$ and a corresponding crossover, when the PAT-rate reaches the standard cotunneling rate.

In conclusion our theory for the generator/detector setup shows standard cotunneling for low generator bias and photon assisted tunneling for high generator bias, where the crossover depends on the effective energy gap of the detector. For weak generator-detector coupling our results agree perfectly with a $P(E)$ -analysis, treating the generator as an environment of the detector. While the relative effect is strong — PAT current is of the same order as the standard cotunneling current — the overall currents are quite small. Stronger coupling yields higher currents, but now new effects contribute to the PAT-rate and the current can not be calculated by $P(E)$ -theory anymore.

Recently a few other systems have been suggested and used as on-chip measurement devices for finite frequency current and/or voltage noise: a single⁵³ or double quantum dot,⁴⁹ a superconducting qubit,⁵⁴ a tunnel junction, both in the normal and superconducting state.^{55,56,57,58,59,60} We have shown that the normal state SET can also function as a finite-frequency noise detector.

V. SUMMARY AND CONCLUSIONS

In this paper we extended the real-time diagrammatics of Ref. 34 to model transport through metallic multi-island systems. We discussed our approach to automatically generate and compute diagrams in executing a systematic perturbation expansion up to second order in the tunneling conductance. This corresponds to sequential and cotunneling terms. Convergence properties of the perturbative expansion were analyzed.

In a setup of two coupled SETs, we demonstrated the importance of cotunneling involving both islands, where energy can be exchanged in between the two tunneling processes. This is linked to the notion of photon assisted tunneling. We performed a $P(E)$ -analysis, treating one SET as an environment for the other one and found excellent agreement between both approaches in the relevant weak coupling limit. In this regime one SET works as a detector of the finite frequency charge noise of the other SET.

Acknowledgments

We acknowledge helpful discussions with R. Schäfer and financial support by DFG via Graduiertenkolleg 276.

APPENDIX A: CALCULATING DIAGRAMS

In this Appendix we explain, how integral expressions, corresponding to the diagrams created, are efficiently calculated. First of all the number of expressions we have to evaluate can be reduced by identifying several distinct types, only differing in some parameters. For these small number of terms numerical and analytical methods of automated calculation are discussed.

1. Reducing denominators

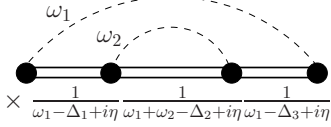
The general structure of integral expressions for a diagram follows easily from the diagrammatic rules discussed above. A self-energy diagram of order R features R integrals over contraction line energies ω_r with corresponding rate functions $\alpha^{j\pm}(\omega_r)$ but also $(2R - 1)$ denominator factors $[\Delta E + i\eta]^{-1}$ for each segment in between two vertices. The workhorse for evaluating these expressions is Cauchy's formula:

$$\frac{1}{x + i\eta} = P \frac{1}{x} - i\pi\delta(x), \quad (\text{A1})$$

which obviously can only be used, when integrating over the variable x . Consequently we have to reduce the number of denominator terms from $(2R - 1)$ to R . Note here, that Cauchy's formula can still be applied to higher-order poles:

$$\frac{1}{(x + i\eta)^2} = -\frac{d}{dx} \frac{1}{x + i\eta} = -\frac{d}{dx} \left[P \frac{1}{x} - i\pi\delta(x) \right]. \quad (\text{A2})$$

$$(a) \quad \int d\omega_1 \alpha_1(\pm\omega_1) \int d\omega_2 \alpha_2(\pm\omega_2)$$



$$(b) \quad \int d\omega_1 \alpha_1(\pm\omega_1) \int d\omega_2 \alpha_2(\pm\omega_2)$$

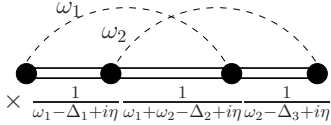


FIG. 6: Two topologically distinct types of diagrams are found. This yields four different integral terms, to be evaluated.

While this reduction is possible for arbitrary order, we will illustrate it for second order diagrams only. As illustrated in Fig. 6, there are two topologically distinct diagrams, depending on, whether the first vertex is connected to third or fourth vertex. Note, that the position of vertices on upper or lower branch is irrelevant for the general structure of the analytical expressions, which are indicated in Fig. 6. Elementary algebraic manipulation of the denominator factors – merely the treatment of infinitesimal η requires some care – yields four expressions with the number of denominator factors reduced as required.

From the first expression (a) we get:

$$\frac{1}{\omega_1 - \Delta_1 + i\eta} \frac{1}{\omega_1 + \omega_2 - \Delta_2 + i\eta} \frac{1}{\omega_1 - \Delta_3 + i\eta}$$

$$= \begin{cases} \Delta_1 = \Delta_3 & : \frac{d}{d\Delta_1} \frac{1}{\omega_1 - \Delta_1 + i\eta} \frac{1}{\omega_1 + \omega_2 - \Delta_2 + i\eta} \\ \Delta_1 \neq \Delta_3 & : \frac{1}{\Delta_1 - \Delta_3} \frac{1}{\omega_1 + \omega_2 - \Delta_2 + i\eta} \\ & \times \left(\frac{1}{\omega_1 - \Delta_1 + i\eta} - \frac{1}{\omega_1 - \Delta_3 + i\eta} \right) \end{cases}.$$

Correspondingly (b) yields:

$$\frac{1}{\omega_1 - \Delta_1 + i\eta} \frac{1}{\omega_1 + \omega_2 - \Delta_2 + i\eta} \frac{1}{\omega_2 - \Delta_3 + i\eta}$$

$$= \begin{cases} \Delta_1 + \Delta_3 = \Delta_2 & : \frac{d}{d\Delta_2} \frac{1}{\omega_1 + \omega_2 - \Delta_2 + i\eta} \\ & \times \left(\frac{1}{\omega_1 - \Delta_1 + i\eta} + \frac{1}{\omega_2 - \Delta_3 + i\eta} \right) \\ \Delta_1 + \Delta_3 \neq \Delta_2 & : \left(\frac{1}{\omega_1 + \omega_2 - \Delta_1 - \Delta_3 + i\eta} \right. \\ & \left. - \frac{1}{\omega_1 + \omega_2 - \Delta_2 + i\eta} \right) \frac{1}{\Delta_1 + \Delta_3 - \Delta_2} \\ & \times \left(\frac{1}{\omega_1 - \Delta_1 + i\eta} + \frac{1}{\omega_2 - \Delta_3 + i\eta} \right) \end{cases}$$

for the second topologically distinct type.

2. Mirror rule

Further simplifications arise from an inherent symmetry property of the diagrammatic rules. From the construction principles for diagrams it is easily seen, that, starting from any diagram, we will obtain another possible diagram by the following operation:

Reflect the diagram along a horizontal line, whereby exchanging forward and backward branch of the contour and change the direction of all tunneling lines. The charge state for any part of the contour then remains unchanged. Both diagrams contribute to the same matrix entry of the self-energy, as only the diagonal part of Σ has to be considered. Application of the diagrammatic rules shows, that merely the energies in the denominator terms change sign:

$$\frac{1}{\Delta E + i\eta} \rightarrow \frac{1}{-\Delta E + i\eta} = - \left(\frac{1}{\Delta E + i\eta} \right)^*, \quad (A3)$$

resulting in cancellation of the real parts of the two mirrored diagrams. Consequently we only calculate the imaginary part of each diagram. This allows to utilize the δ -function part of Cauchy's formula for evaluating one of the two integrations. Our problem reduces then to the calculation of a single (principal value) integral, where the resulting integrand can be written as a product of one or two rate functions – there might be a derivative acting on one of them – multiplied with the principal value term $P\frac{1}{\omega}$.

3. Evaluating the integrals

Above (see Eqn. 10) we calculated analytical expressions for the rate functions for the case of normal reservoirs with a constant density of states (DOS) and equal temperatures for both sides of the tunneling barrier. It is interesting, though, that important general features of the rate functions will persist, if these conditions are relaxed, e.g. for non-equal temperatures, relevant for considering thermopower or self-heating effects, or for tunneling rates of quasiparticles in superconducting devices, where the gapped BCS density of states enters. Common to all these cases, however, is the existence of a certain onset-energy, where the asymptotic behavior is linear on one, vanishing on the other side of this threshold; the asymptotic convergence is hereby governed by some Boltzmann factor.

Evidently, a high-energy cutoff is needed for convergence of integrals, where the two rate functions grow in the same direction. This cutoff is provided for in a natural way by the bandwidth of the reservoirs, as a more careful analysis of the rate function for a DOS limited to some finite bandwidth reveals. The cutoff will at most enter logarithmically into any final result – indeed, for the single SET it is known to drop out completely from the measurable quantities current and average charge. Hence, there is no need for a microscopically

detailed derivation of a specific cutoff function and we can choose for convenience of calculation a Breit-Wigner factor centered around the onset.

An *analytical* solution of the integrals is then possible for the rate functions as given in Eqn. 10. Contour integration leads to sums over Matsubara-frequencies, which in turn results in analytical expressions involving Digamma-functions, where the onset-energies enter as parameters (cf. Ref. 29).

Since further algebraic manipulation of these complex terms is not feasible for multi-island geometries, it can be more convenient to adopt a *numerical* approach, already for calculating the integrals – the additional benefit being, that this approach is also capable of dealing with the alternative rate functions discussed above effortlessly. Numerical evaluation is helped by the general features shared by all these rate functions. They allow for precise numerical integration for a small region (of a few $k_B T$) around the onset, while the asymptotics can be trivially integrated analytically.

APPENDIX B: CONVERGENCE OF A PERTURBATIVE EXPANSION

In this Appendix we address the question of the applicability range of our perturbation expansion. To motivate a criterion for general multi-island systems let us first consider the case of a single SET. In this case, we have a *non-perturbative* result for the current within the so-called resonant tunneling approximation (RTA)³⁴ at hand:

$$I^{\text{sd}} = \frac{2\pi e}{\hbar} \int d\omega \alpha_L(\omega) \alpha_R(\omega) |\Pi(\omega)|^2 [f_L^+(\omega) - f_R^+(\omega)], \quad (\text{B1})$$

where $\alpha_r = \alpha_r^+ + \alpha_r^-$ and the propagator $\Pi(\omega) = [\omega - \Delta - \sigma(\omega)]^{-1}$ dressed with first order transitions as exemplified in the self-energy

$$\begin{aligned} \text{Re } \sigma(\omega) &= -2 \sum_r \alpha_0^r (\omega - \mu_r) & (\text{B2}) \\ &\times \left[\ln \left(\frac{\beta E_C}{2\pi} \right) - \text{Re } \Psi \left(\frac{i\beta(\omega - \mu_r)}{2\pi} \right) \right] \end{aligned}$$

$$\text{Im } \sigma(\omega) = -\pi \sum_r \alpha_r^r (\omega), \quad (\text{B3})$$

where the cut-off energy E_C is of the order of the charging energy. We see that the dominant contribution to the current comes from energies around the charging energy Δ . Higher-order quantum fluctuations embodied by $\sigma(\omega)$ both shift (real part) and broaden (imaginary part) the region of contributing energies.

For definiteness we consider now the scenario $\mu_L - \mu_R = eV > 0$, where we are interested in the onset of sequential tunneling around $\mu_L \lesssim \Delta$, while a finite bias $eV \gg k_B T$ is applied asymmetrically across the SET. The main contribution to the current in this regime is then given by electrons slowly tunneling onto the island from the left lead (the rate for this bottleneck process being $\alpha_L^+(\omega)$, while they quickly tunnel off to the right lead ($\alpha_R^-(\omega) \gg \alpha_L^+(\omega)$)). Consequently the

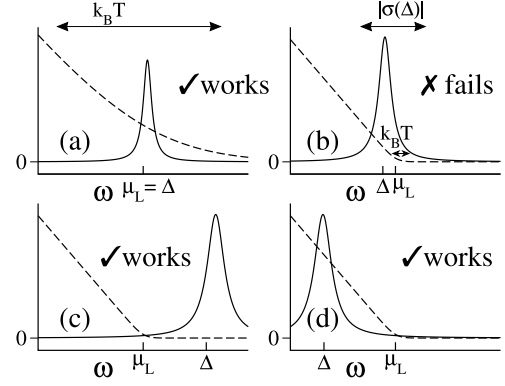


FIG. 7: Sketch of $\alpha_L^+(\omega)$ (broken line) and $\text{Im } \Pi(\omega)$ (solid line) in the integrand of Eqn. B4. Perturbative expansion works, if the rate α_L^+ is approximately linear in the region given by the peak in $\text{Im } \Pi(\omega)$, corresponding to $|\sigma(\Delta)| < k_B T$ on resonance (a) or to $|\Delta - \mu_L| > |\sigma(\Delta)|$ in (c) and (d). The expansion fails (b) for $\text{Im } \Pi(\omega)$ incorporating the kink in α_L^+ .

current (Eqn. B1) simplifies to:

$$I^{\text{sd}} = -\frac{2e}{\hbar} \text{Im} \int d\omega \frac{\alpha_L^+(\omega)}{\omega - \Delta - \sigma(\omega)}, \quad (\text{B4})$$

where the imaginary part of the self-energy, the lifetime width of the resonant level, is dominated by the (decay) rate for tunneling out to the right lead.

To understand the effect of a systematic perturbation expansion of the current operator, as performed in the main part of the paper, we expand now this expression for the current (Eqn. B4) in orders of the tunneling conductance α_0 . Expansion of the denominator yields:

$$\begin{aligned} \frac{1}{\omega - \Delta - \sigma(\omega)} &= \frac{1}{\omega - \Delta + i\eta} & (\text{B5}) \\ &+ \frac{\sigma(\omega)}{(\omega - \Delta + i\eta)^2} + \frac{1}{2} \frac{\sigma(\omega)^2}{(\omega - \Delta + i\eta)^3} + \dots, \end{aligned}$$

where the denominator terms are regularized by infinitesimal imaginary parts. This should be construed in terms of the Cauchy-identity for generalized functions and derivatives thereof (Eqns. A1 and A2).

The term of this expansion of order α_0^n contains the denominator $(\omega - \Delta + i\eta)^{-(n+1)}$, which results in a n^{th} derivative of a δ -function. Within the integral expression for the current (Eqn. B4) we will use partial integration, so that the derivatives act on $\alpha_L^+(\omega) \sigma(\omega)^n$. The expansion in terms of α_0 therefore correspond to a Taylor-expansion around the bare resonance Δ . In Fig. 7 we visualize the integration of Eqn. B4 for different parameter regimes. We integrate the rate function $\alpha_L^+(\omega)$, which has a kink at $\omega = \mu_L$ with a characteristic width of $k_B T$, multiplied with $\text{Im } \Pi(\omega)$, which is peaked close to Δ , shifted by $|\text{Re } \sigma(\omega)|$ and has a width given by $|\text{Im } \sigma(\omega)|$.

As just shown the perturbation expansion consists of expanding the peak of $\text{Im } \Pi(\omega)$ in terms of derivatives of δ -functions, consequently capturing properties of $\alpha_L^+(\omega)$ (and its derivatives) at Δ only.

As is intuitively clear from Figs. 7 (a)–(d), this will work, if the peak $\text{Im}\Pi(\omega)$ is sharp, as compared to the structure in $\alpha_L^+(\omega)$ in the relevant regime. This means that either $|\sigma(\Delta)|$ has to be smaller than $k_B T$ for considering the system on resonance $\Delta = \mu_L$ (Fig. 7 (a)) or that the expansion takes place so far away from resonance with the left lead, that the peak $\text{Im}\Pi(\omega)$ is not incorporating the kinked region of $\alpha_L^+(\omega)$; i.e., $|\Delta - \mu_L| > |\sigma(\Delta)|$ (see Fig. 7 (c) and (d)). Then the rate function is expanded in the asymptotic region, where it is exponentially suppressed (c) or rising approximately linearly (d). Consequently higher order derivatives from higher order terms of the expansion in α_0 do not contribute and second order perturbation theory suffices.

We can formalize these intuitive arguments by considering the Taylor-expansion of the bottleneck rate, resulting from the derivatives of the δ -function in the perturbative expansion (Eqn. B6):

$$\frac{\alpha_0^L \omega}{\exp(\beta\omega) - 1} = \alpha_0^L \left(\frac{1}{\beta} + \frac{\omega}{2} + \frac{\beta\omega^2}{6 \cdot 2!} - \frac{\beta^3\omega^4}{30 \cdot 4!} + \dots \right).$$

Note the increasing powers of the inverse temperature β , endangering convergence for low temperatures. The largest term now to appear in the n^{th} term of the α_0 expansion is a term with magnitude:

$$\partial_\omega^{n-1} \alpha_L^+(\omega) \sigma(\omega)^{n-1} \propto \alpha_0^L \beta^{n-2} [\sigma(\Delta)]^{n-1},$$

where all derivatives have acted on $\alpha_L^+(\omega)$.⁶¹ Correspond-

ingly we get a series in the parameter $\beta |\sigma(\Delta)|$, which has to be small for convergence, confirming our argument above.

In summary, we found a criterion for the applicability range of second-order perturbation theory. The ideas developed by considering a single SET can be easily generalized to an arbitrary multi-island geometry. For each island, all tunneling rates should be approximately linear in the region of the contributing energies. This leads to the condition

$$\max\{k_B T, |\Delta - \mu_j|\} > |\sigma(\Delta)|, \quad (\text{B6})$$

where $\sigma(\Delta)$ is the self energy characterizing shift and width of the resonance due to quantum fluctuations. For $k_B T > \sigma(\Delta)$ the tunneling rate is approximately linear on the relevant scale of integration, while for $|\Delta - \mu_j| > \sigma(\Delta)$ the kink in the rate function is outside the integration region, and consequently the rate is either linear or exponentially small.

An example of the failure of perturbative expansion is an SET at finite bias and low temperature. Likewise in a setup of two islands in series²¹ the resonance is shifted by a self-energy scaling as: $\text{Re } \sigma \propto \alpha_0 E_C$, not vanishing for aligned levels of the two islands. This can result in a failure of perturbative expansion at low temperatures.⁸

No problems are encountered for the scenario laid out in Sec. IV. Here the generator SET is completely dominated by sequential tunneling, while the detector, biased on the order of temperature, correspondingly yields a small $|\sigma(\Delta)| \approx \alpha_0 k_B T$ fulfilling Eqn. B6.

¹ T. A. Fulton and G. J. Dolan, Phys. Rev. Lett. **59**, 109 (1987).
² O. Kulik and R.I. Shekhter, Sov. Phys. JETP **41**, 308 (1975).
³ D.V. Averin and K. K. Likharev, J. Low Temp. Phys. **62**, 345 (1986).
⁴ *Single Charge Tunneling*, NATO ASI Series **294**, H. Grabert and M. H. Devoret, eds., (Plenum Press, New York, 1992).
⁵ M. Amman, E. Ben-Jacob, and K. Mullen, Phys. Lett. A **142**, 431 (1989).
⁶ D. V. Averin, A. N. Korotkov, and Yu. V. Nazarov, Phys. Rev. Lett. **66**, 2818 (1991).
⁷ A. N. Korotkov, Phys. Rev. B **50**, 17674 (1994).
⁸ T. Pohjola, J. König, H. Schoeller, and G. Schön, Phys. Rev. B **59**, 7579 (1999).
⁹ D. Esteve, in *Single Charge Tunneling* (Ref. 4), p. 109.
¹⁰ R. Schäfer, B. Limbach, P. vom Stein, C. Wallisser, Physica E **18**, 87 (2003).
¹¹ K. W. Lehnert, B. A. Turek, K. Bladh, L. F. Spietz, D. Gunnarsson, P. Delsing, and R. J. Schoelkopf, Phys. Rev. Lett. **91**, 106801 (2003).
¹² B. A. Turek, K. W. Lehnert, A. Clerk, D. Gunnarsson, K. Bladh, P. Delsing, and R. J. Schoelkopf, Phys. Rev. B **71**, 193304 (2005).
¹³ L. S. Kuzmin, P. Delsing, T. Claeson, and K. K. Likharev, Phys. Rev. Lett. **62**, 2539 (1989).
¹⁴ H. Pothier, P. Lafarge, P. F. Orfila, C. Urbina, D. Esteve, and M. H. Devoret, Physica B **169**, 573 (1991).
¹⁵ C. Urbina, H. Pothier, P. Lafarge, P. F. Orfila, D. Esteve, M. Devoret, L. J. Geerligs, V. F. Anderegg, P. A. M. Holweg, and J. E. Mooij, IEEE Trans. Magn. **27**, 2578 (1991).
¹⁶ J. P. Pekola, K. P. Hirvi, J. P. Kauppinen, and M. A. Paalanen, Phys. Rev. Lett. **73**, 2903 (1994).
¹⁷ R. L. Kautz, M. W. Keller, and J. M. Martinis, Phys. Rev. B **60**, 8199 (1999).
¹⁸ N. M. Zimmerman and M. W. Keller, Meas. Sci. Technol. **14**, 1237 (2003).
¹⁹ H. Scherer, S. V. Lotkhov, G.-D. Willenberg, and A. B. Zorin, cond-mat/0412240 (unpublished).
²⁰ J. Bylander, T. Duty, and P. Delsing, Nature **434**, 361 (2005).
²¹ B. Limbach, P. vom Stein, C. Wallisser, and R. Schäfer, Phys. Rev. B **72**, 045319 (2005).
²² K. K. Likharev, IEEE Trans. Mag. **23**, 1142 (1987).
²³ D. V. Averin and A. A. Odintsov, Phys. Lett. A **140**, 251 (1989).
²⁴ D. V. Averin and Yu. V. Nazarov, Phys. Rev. Lett. **65**, 2446 (1990).
²⁵ H. D. Jensen and J. M. Martinis, Phys. Rev. B **46**, 13407 (1992).
²⁶ K. A. Matveev, Sov. Phys. JETP **72**, 892 (1991), [Zh. Eksp. Teor. Fiz. **99**, 1598 (1991)].
²⁷ P. Joyez, V. Bouchiat, D. Esteve, C. Urbina, and M. H. Devoret, Phys. Rev. Lett. **79**, 1349 (1997).
²⁸ C. Wallisser, B. Limbach, P. vom Stein, R. Schäfer, C. Theis, G. Göppert, and H. Grabert, Phys. Rev. B **66**, 125314 (2002).
²⁹ J. König, H. Schoeller, and G. Schön, Phys. Rev. Lett. **78**, 4482 (1997); Phys. Rev. B **58**, 7882 (1998).
³⁰ D.S. Golubev and A.D. Zaikin, Pis'ma Zh. Eksp. Teor. Fiz. **63**, 953 (1996) [JETP Lett. **63**, 1007 (1996)].
³¹ G. Göppert and H. Grabert, Phys. Rev. B **58**, R10155 (1998).
³² J. König and H. Schoeller, Phys. Rev. Lett. **81**, 3511 (1998).
³³ G. Göppert, B. Hüpper, and H. Grabert, Phys. Rev. B **62**, 9955

(2000).

³⁴ H. Schoeller and G. Schön, Phys. Rev. B **50**, 18436 (1994); J. König, H. Schoeller, and G. Schön, Europhys. Lett. **31**, 31 (1995).

³⁵ P. Lafarge and D. Esteve, Phys. Rev. B **48**, 14309 (1993).

³⁶ L. R. C. Fonseca, A. N. Korotkov, K. K. Likharev, and A. A. Odintsov, J. Appl. Phys. **78** (1995).

³⁷ C. Wasshuber, "Computational Single-Electronics", Springer-Verlag, ISBN 3-211-83558-X (2001).

³⁸ A. Thielmann, M. H. Hettler, J. König, and G. Schön, Phys. Rev. Lett. **95**, 146806 (2005); A. Braggio, J. König, and R. Fazio, cond-mat/0507527 (unpublished).

³⁹ We restrict our formulation here to geometries without direct junctions between two leads and each lead is connected to one island only.

⁴⁰ W. G. van der Wiel, S. De Franceschi, J. M. Elzerman, T. Fujisawa, S. Tarucha, and L. P. Kouwenhoven, Rev. Mod. Phys. **75**, 1 (2003).

⁴¹ The charge state can be treated as independent from the fermionic degrees of freedom connected to field operators $a_{l_j\lambda\mathbf{v}}, a_{l_j\lambda\mathbf{v}}^\dagger, c_{m_j\lambda\mathbf{v}}, c_{m_j\lambda\mathbf{v}}^\dagger$ as the total number of electrons on any island is large.

⁴² H. Schoeller, in Mesoscopic Electron Transport, edited by L. L. Sohn, L. P. Kouwenhoven, and G. Schön (Kluwer Academic Press, The Netherlands, 1997).

⁴³ The line direction is to be understood as taken with respect to the convention for the direction of a junction as chosen above.

⁴⁴ Charge states, neighboring the chosen subspace might appear in these intermediate step, which charging energies hence are also needed.

⁴⁵ According to this systematic expansion the second order current contribution includes not only higher order transition rates ($P_{\chi'}^{(0)}\Sigma_{\chi'\chi}^{(2)}$) but also higher order corrections to the stationary probability $P_{\chi'}^{(1)}\Sigma_{\chi'\chi}^{(1)}$.

⁴⁶ M. Meschke, J. P. Pekola, F. Gay, R. E. Rapp, and H. Godfrin, J. Low Temp. Phys. **134**, 1119 (2004).

⁴⁷ D. C. Dixon, C. P. Heij, P. Hadley, and J. E. Mooij, J. Low Temp. Phys. **118**, 325 (2000).

⁴⁸ G.-L. Ingold and Yu. V. Nazarov, in *Single Charge Tunneling* (Ref. 4), p. 21.

⁴⁹ R. Aguado and L. P. Kouwenhoven, Phys. Rev. Lett. **84**, 1986 (2000).

⁵⁰ G. Johansson, P. Delsing, K. Bladh, D. Gunnarsson, T. Duty, A. Käck, G. Wendin, and A. Aassime in *Quantum Noise in Mesoscopic Physics* edited by Y. V. Nazarov (Kluwer Academic Publishers, The Netherlands, 2003).

⁵¹ G. Johansson, A. Käck, and G. Wendin, Phys. Rev. Lett. **88**, 046802 (2002).

⁵² A. Käck, G. Wendin, and G. Johansson, Phys. Rev. B **67**, 035301 (2003).

⁵³ F. Balestro, E. Onac, L. W. van Beveren, R. Hanson, U. Hartmann, Yu. V. Nazarov, and L. P. Kouwenhoven (unpublished)

⁵⁴ R. J. Schoelkopf, A. A. Clerk, S. M. Girvin, K. W. Lehnert, and M. H. Devoret, in *Quantum Noise in Mesoscopic Physics* edited by Yu. V. Nazarov (Kluwer Academic Publishers, The Netherlands, 2003).

⁵⁵ R. Deblock, E. Onac, L. Gurevich, L. P. Kouwenhoven, Science **301**, 203 (2003).

⁵⁶ J. Tobiska and Yu. V. Nazarov, Phys. Rev. Lett. **93**, 106801 (2004).

⁵⁷ E. B. Sonin, Phys. Rev. B **70**, 140506(R) (2004).

⁵⁸ R. K. Lindell, J. Delahaye, M. A. Sillanpää, T. T. Heikkilä, E. B. Sonin, and P. J. Hakonen, Phys. Rev. Lett. **93**, 197002 (2004).

⁵⁹ J. P. Pekola, Phys. Rev. Lett. **93**, 206601 (2004).

⁶⁰ T. T. Heikkilä, P. Virtanen, G. Johansson, and F. K. Wilhelm, Phys. Rev. Lett. **93**, 247005 (2004).

⁶¹ For completeness we note, that the analyzed term, endangering convergence of the series, is not necessarily the largest term, as the principal value parts from the denominators $(\omega - \Delta + i\eta)^{-(n+1)}$ may gain importance. Consider, e.g., standard cotunneling deep in the cotunneling regime, i.e., in the exponentially suppressed region of the rate $|\Delta - \mu_L| > |\sigma(\Delta)|, k_B T$. There second order terms (stemming from those principal value parts) being algebraically suppressed dominate over exponentially suppressed first-order contributions. Nonetheless the convergence argument from above is fulfilled and, indeed, higher than second-order contributions are sufficiently small.